JOURNAL OF GEOPHYSICAL RESEARCH, VOL. 102, NO. D14, PAGES 16,831–16,847, JULY 27, 1997

Modeling phase functions for dustlike tropospheric aerosols using a shape mixture of randomly oriented polydisperse spheroids

Michael I. Mishchenko

NASA Goddard Institute for Space Studies, New York, and Institute of Terrestrial and Planetary Atmospheres/State University of New York at Stony Brook

Larry D. Travis

NASA Goddard Institute for Space Studies, New York

Ralph A. Kahn and Robert A. West

Jet Propulsion Laboratory, California Institute of Technology, Pasadena

Abstract. Laboratory and in situ measurements show that scattering properties of natural nonspherical particles can be significantly different from those of volume- or surface-equivalent spheres, thus suggesting that Mie theory may not be suitable for interpreting satellite reflectance measurements for dustlike tropospheric aerosols. In this paper we use the rigorous *T*-matrix method to extensively compute light scattering by shape distributions of polydisperse, randomly oriented spheroids with refractive indices and size distributions representative of naturally occurring dust aerosols. Our calculations show that even after size and orientation averaging, a single spheroidal shape always produces a unique, shape-specific phase function distinctly different from those produced by other spheroidal shapes. However, phase functions averaged over a wide aspect-ratio distribution of prolate and oblate spheroids are smooth, featureless, and nearly flat at side-scattering angles and closely resemble those measured for natural soil and dust particles. Thus, although natural dust particles are, of course, not perfect spheroids, they are always mixtures of highly variable shapes, and their phase function can be adequately modeled using a wide aspect-ratio distribution of prolate and oblate spheroidal grains. Our comparisons of nonspherical versus projected-area-equivalent spherical particles show that spherical-nonspherical differences in the scattering phase function can be large and therefore can cause significant errors in the retrieved aerosol optical thickness if Mie theory is used to analyze reflectance measurements of nonspherical aerosols. On the other hand, the differences in the total optical cross sections, single-scattering albedo, asymmetry parameter of the phase function, and backscattered fraction are much smaller and in most cases do not exceed 10%. This may suggest that for a given aerosol optical thickness the influence of particle shape on the aerosol radiative forcing is negligibly small. Spherical-nonspherical differences in the extinction-to-backscatter ratio are very large and should be explicitly taken into account in inverting lidar measurements of dustlike aerosols.

1. Introduction

Tropospheric aerosols are thought to cause a significant direct and indirect climate forcing, but the magnitude of this forcing remains highly uncertain because of poor knowledge of global aerosol characteristics and temporal changes [*Hansen and Lacis*, 1990; *Charlson et al.*, 1992; *Lacis and Mishchenko*, 1995; *Hansen et al.*, 1995]. The retrieval of the global distribution of the aerosol optical depth and aerosol physical and optical properties is one of the key objectives of several planned spacecraft instruments such as the moderate resolution imaging spectrometer (MODIS) [*King et al.*, 1992], multi-angle imaging spectro-radiometer (MISR) [*Diner et al.*, 1991], earth observing scanning polarimeter (EOSP) [*Travis*, 1992], and the polarization and directionality of the earth's reflectances (POLDER) instrument [*Deschamps et al.*, 1994]. The first three instruments are part of the NASA's Earth Observing System, while POLDER is scheduled to fly on the Japanese Advanced Earth Observing Satellite (ADEOS). It is now well realized that the quality of the optical thickness retrievals based on analyzing reflectance data critically depends on the accuracy of modeling the aerosol phase function and single-scattering albedo [*Wang and Gordon*, 1994]. In this regard, a special

Copyright 1997 by the American Geophysical Union.

Paper number 96JD02110.
0148-0227/97/96JD-02110$09.00

problem is posed by dustlike tropospheric aerosols, since their predominantly nonspherical shapes can make the standard Mie theory not applicable to computing their scattering properties [*Heintzenberg*, 1978; *Koepke and Hess*, 1988; *Kaufman*, 1993; *von Hoyningen-Huene and Wendisch*, 1994; *Mishchenko et al.*, 1995; *Kahn et al.*, this issue]. Indeed, many laboratory and in situ measurements show that scattering properties of natural nonspherical particles can be significantly different from those of equivalent spheres [*Perry et al.*, 1978; *Jaggard et al*, 1981; *Nakajima et al.*, 1989; *Kuik*, 1992; *West et al.*, this issue]. Unfortunately, the arrangement of source of light and detector usually precludes laboratory measurements at scattering angles close to 0° and 180°. This makes experimental determinations of the scattering cross section, single-scattering albedo, and phase function very difficult and greatly enhances the importance of accurate theoretical modeling of nonspherical scattering. Therefore it is the primary goal of this theoretical paper to provide a better representation of dustlike aerosol scattering properties in the framework of satellite aerosol retrieval algorithm development.

In order to be realistic, theoretical computations of light scattering by ensembles of natural nonspherical aerosols must address the distribution of particles over sizes and orientations [*Wiscombe and Mugnai*, 1988; *Mishchenko et al.*, 1996a]. Furthermore, microphotographs of natural aerosols show a great variety of shapes [*Okada et al.*, 1987; *Nakajima et al.*, 1989; *Guieu et al.*, 1994], thus making questionable the ability of a single nonspherical shape to represent scattering properties of the natural shape mixture. Indeed, recent theoretical studies of nonspherical scattering have demonstrated that even after size and orientation averaging, essentially any particle shape, either regular or irregular, produces its own, shape-specific scattering pattern. Two well-known examples are provided by halos produced by single or aggregated hexagonal particles [*Takano and Liou*, 1989; *Macke*, 1993] and by rainbows produced by spheres [*Hansen and Travis*, 1974]. Other examples of shape-specific phase functions can be found in the work by *Muinonen et al.* [1989] and *Macke et al.* [1996]. In contrast, laboratory and in situ measurements for natural ensembles of nonspherical particles show that in most cases, phase functions are relatively smooth and featureless, especially at side-scattering angles [*Perry et al.*, 1978; *Jaggard et al.*, 1981; *Nakajima et al.*, 1989; *Kuik*, 1992; *Francis*, 1995; *Posse and von Hoyningen-Huene*, 1995; *Gayet et al.*, 1995; *West et al.*, this issue]. This smooth scattering-angle dependence can be explained by natural particle ensembles being mixtures of different shapes in which shape-specific details of individual phase functions are averaged out [*Wiscombe and Mugnai*, 1986; *Bohren and Singham*, 1991].

At present, the only technique potentially capable of accurately computing light scattering by small arbitrarily shaped particles is the discrete dipole approximation [*Draine and Flatau*, 1994; *Lumme and Rahola*, 1994]. Unfortunately, this technique becomes very time consuming when particle size parameters exceed 5 and, especially, when averaging over particle sizes, shapes, and orientations is required. As a result, the use of the discrete dipole approximation in application to realistic shape distributions of polydisperse, randomly oriented dustlike aerosols is currently impractical.

Another method widely used for rigorously computing light scattering by nonspherical particles is the *T*-matrix approach [*Waterman*, 1971]. This method has been substantially improved recently [*Mishchenko*, 1991; *Mishchenko and Travis*, 1994a; *Wielaard et al.*, 1997] and now allows computations for randomly oriented particles with size parameters well exceeding 50. In application to randomly oriented particles this method can be many orders of magnitude faster than the discrete dipole approximation, allows the use of moderate scientific workstations, and is ideally suited to compute light scattering by realistic size distributions of nonspherical aerosols. The only disadvantage of essentially all currently available *T*-matrix codes is that they have been specifically developed to compute light scattering by rotationally symmetric nonspherical particles such as spheroids [*Mishchenko et al.*, 1996a], finite circular cylinders [*Kuik et al.*, 1994; *Mishchenko et al.*, 1996b], and Chebyshev particles [*Wiscombe and Mugnai*, 1986; *Mugnai and Wiscombe*, 1986; *Wiscombe and Mugnai*, 1988]. As a consequence, the natural question arises as to the ability of a mixture of such simple shapes to adequately reproduce scattering properties of natural nonspherical aerosols. *Hill et al.* [1984] have suggested that the scattering phase function of natural soil particles can be represented by a size/shape mixture of randomly oriented spheroids much better than by projected-area-equivalent spheres. However, this result was based on computations for only 37 different spheroids in random orientation. The recent significant improvements of the *T*-matrix method have made possible a much more detailed study. Therefore, in this paper we reexamine the conclusion of *Hill et al.* [1984] on the basis of extensive *T*-matrix computations for shape mixtures of polydisperse, randomly oriented spheroids. We also discuss the effect of aerosol particle nonsphericity on several scattering characteristics which determine the direct radiative forcing by aerosols and/or are used in aerosol remote sensing.

2. Definitions and Computational Technique

The primary photometric quantities describing the single scattering of a monochromatic light beam by a small-volume element containing randomly oriented nonspherical particles are the ensemble-averaged extinction $C_{\rm ext}$ and scattering $C_{\rm sca}$ cross sections per particle and the phase function P [*van de Hulst*, 1957; *Bohren and Huffman*, 1983]. The phase function describes the angular distribution of the scattered intensity and satisfies the normalization condition

$$\frac{1}{2}\int_0^{\pi} d\Theta \sin\Theta\, P(\Theta) = 1, \qquad (1)$$

where Θ is the scattering angle (angle between the incident and the scattered beams). The optical cross sections and the phase function can be used to define other important scattering characteristics of the small-volume element such as the absorption cross section per particle $C_{\rm abs}$ and single-scattering albedo ϖ:

$$C_{\rm abs} = C_{\rm ext} - C_{\rm sca}, \qquad (2)$$

$$\varpi = \frac{C_{\text{sca}}}{C_{\text{ext}}}. \tag{3}$$

The quantity

$$\langle\cos\Theta\rangle = \frac{1}{2}\int_{-1}^{1} d(\cos\Theta)\,P(\Theta)\cos\Theta \tag{4}$$

is called the asymmetry parameter of the phase function and is positive for particles that scatter predominantly in the forward hemisphere, negative for backscattering particles, and zero for symmetric phase functions with $P(\pi-\Theta) = P(\Theta)$. The backscattered fraction for isotropically incident radiation β is defined as

$$\beta = \frac{1}{2\pi}\int_{0}^{\pi} d\Theta\,P(\Theta)\,\Theta\sin\Theta \tag{5}$$

[*Wiscombe and Grams*, 1976]. This quantity enters the two-stream approximation and is sometimes used to experimentally estimate the asymmetry parameter of the phase function [*Marshall et al.*, 1995]. Finally, the extinction-to-backscatter ratio is defined as

$$R_{\text{eb}} = \frac{C_{\text{ext}}}{C_{\text{sca}}P(180°)} \tag{6}$$

and is widely used in lidar aerosol retrievals [*Reagan et al.*, 1989; *Stephens*, 1994].

The phase function is often represented as a Legendre polynomial expansion [*van de Hulst*, 1980],

$$P(\Theta) = \sum_{n=0}^{n_{\max}} \omega_n\, P_n(\cos\Theta), \tag{7}$$

where $P_n(\cos\Theta)$ are Legendre polynomials, and the value of the upper summation limit $n_{\max}$ depends on the desired numerical accuracy of computations. It is the explicit use of the Legendre expansion that makes our version of the *T*-matrix technique much faster than the traditional approach based on a direct computation of the phase function for a large set of scattering angles [*Mishchenko*, 1991]. The number of numerically significant terms in the expansion of equation (7) is often relatively small, thus making this expansion an ideal numerical representation of the phase function suitable for efficiently computing the phase function for essentially any number of scattering angles with a minimum consumption of CPU time. Using the orthogonality property of Legendre polynomials, we easily derive from equations (4) and (7),

$$\langle\cos\Theta\rangle = \frac{\omega_1}{3}. \tag{8}$$

The integral in equation (5) can be calculated numerically by using the standard Gaussian quadrature formula and efficiently evaluating the phase function values at Gaussian division points via equation (7).

We compute the optical cross sections C_{ext} and C_{sca} and the expansion coefficients ω_n for a shape mixture of polydisperse, randomly oriented spheroids using the *T*-matrix approach. Numerical aspects of the *T*-matrix computations and practical limitations on the maximum particle size parameter and/or particle aspect ratio are discussed in detail by *Wiscombe and Mugnai* [1986], *Mishchenko* [1993], and *Mishchenko and Travis* [1994a]. In averaging the light-scattering characteristics over particle sizes, we must use an aerosol size distribution. Unfortunately, at present there is no clear consensus as to the size distribution best describing natural aerosol polydispersions. Therefore we decided to use in this paper two different size distributions. The first one represents the standard model of the accumulation mode of dustlike aerosols adopted in the MISR aerosol retrieval algorithm [*Diner et al.*, 1994] and given by

$$n(r) = \frac{C_1}{r}\exp\left[-\frac{(\ln r-\ln r_g)^2}{2\ln^2\sigma_g}\right] \qquad 0.05\,\mu\text{m} \le r \le 2\,\mu\text{m}, \tag{9}$$

where r is the radius (for spherical particles) or radius of the equal-projected-area sphere (for spheroids), $n(r)dr$ is the fraction of particles with radii between r and $r + dr$, r_g is the geometric mean radius equal to 0.47 μm, σ_g is the geometric standard deviation equal to 2.51, and the constant C_1 is chosen such that $n(r)$ satisfies the normalization condition

$$\int_{r_{\min}}^{r_{\max}} dx\,n(x) = 1 \tag{10}$$

with $r_{\min}$ = 0.05 μm and $r_{\max}$ = 2 μm. Note that the distribution given by equation (9) differs from the standard lognormal distribution by having explicit lower and upper limits on particle radii instead of allowing the full range of radii from 0 to ∞. This is done, in part, to avoid a physically unrealistic dependence of the optical cross sections and the phase function on "phantom" large particles that are implicitly contained within the large particle tail of the standard lognormal distribution with a large geometric standard deviation [e.g., *Lacis and Mishchenko*, 1995]. The second size distribution used here is the power law distribution given by [*Toon and Pollack*, 1976; *Lenoble and Brogniez*, 1984]

$$n(r) = \begin{cases} C_2 & r \le r_1, \\ C_2\left(r_1/r\right)^3 & r_1 \le r \le r_2, \\ 0 & r > r_2, \end{cases} \tag{11}$$

where, again, the constant C_2 is chosen such that the distribution is normalized to 1 according to equation (10) with $r_{\min} = 0$ and $r_{\max} = r_2$. Instead of using fixed values of the formal parameters r_1 and r_2, we express them in terms of the effective radius and effective variance of the distribution as described below.

It is important to emphasize that in this paper, we characterize the size of a spheroid using the radius of the equal-projected-area sphere or, equivalently, the radius of the equal-surface-area sphere [*van de Hulst*, 1957]. Thus we compare scattering and absorption properties of spherical and nonspherical particles with the same average projected or surface area. Equal-projected-area spheres are often

considered an appropriate substitute for randomly oriented nonspherical particles with sizes much larger than the wavelength of the incident light because the diffraction component of the scattering phase function and the extinction cross section depend primarily on the average projected area [*van de Hulst*, 1957; *Hansen and Travis*, 1974]. It should be kept in mind, however, that scattering and absorption properties of particles much smaller than the wavelength depend primarily on particle volume rather than on particle surface or average projected area [*van de Hulst*, 1957; *Bohren and Huffman*, 1983]. In the latter case a better replacement for randomly oriented nonspherical particles may be provided by equal-volume spheres (see below).

Hansen and Travis [1974] (see also *Hansen and Hovenier* [1974] and *Lacis et al.* [1992]) have demonstrated that the primary characteristics of essentially any physically plausible size distribution of spherical particles are the cross-section-area weighted effective radius given by

$$r_{\text{eff}} = \frac{1}{G} \int_{r_{\min}}^{r_{\max}} dr r \pi r^2 n(r) \tag{12}$$

and the effective variance defined as

$$v_{\text{eff}} = \frac{1}{G r_{\text{eff}}^2} \int_{r_{\min}}^{r_{\max}} dr \left(r - r_{\text{eff}}\right)^2 \pi r^2 n(r), \tag{13}$$

where G is the average cross-sectional area:

$$G = \int_{r_{\min}}^{r_{\max}} dr \pi r^2 n(r). \tag{14}$$

This means that different size distributions having the same values of r_{eff} and v_{eff} have similar single-scattering properties. In view of many different analytical parameterizations of natural size distributions suggested in the literature [e.g., *Lenoble and Brogniez*, 1984], this result of Hansen and Travis is important, since it provides a unified classification of all distributions based on only two key parameters. Recently, *Mishchenko and Travis* [1994b] have extended this result to randomly oriented polydisperse spheroids. For the modified lognormal distribution given by equation (9) with $r_g = 0.47$ μm and $\sigma_g = 2.51$, the effective radius is 1.163 μm and the effective variance is 0.168. For the power law distribution given by equation (11), r_{eff} and v_{eff} depend on the formal parameters r_1 and r_2. However, in view of the result of *Hansen and Travis* [1974], it is more convenient to consider r_{eff} and v_{eff} the primary parameters of the size distribution and determine r_1 and r_2 from equations (11)-(13). It is easy to show that for a fixed v_{eff}, $r_1 = p_1 r_{\text{eff}}$ and $r_2 = p_2 r_{\text{eff}}$, where p_1 and p_2 are constant proportionality factors. The values of these factors for several values of the effective variance are given in Table 1. Note that unlike the standard power law distribution employed by *Hansen and Travis* [1974] and *Mishchenko and Travis* [1994b], the distribution of equation (11) does not have a sharp drop to zero at $r = r_1$. We have found that the elimination of the sharp cutoff at $r = r_1$ leads to a (much) smoother behavior of the optical cross sections and the phase function with varying effective radius.

Table 1. Values of the Factors p_1 and p_2 for Several Values of the Effective Variance of the Power Law Size Distribution Given by Equation (11) (See Text)

v_{eff}	p_1	p_2
0.1	0.89031	1.56538
0.2	0.61383	1.94912
0.4	0.37433	2.52160
1	0.11958	3.91046

Microphotographs of naturally occurring dustlike aerosols show a great variability of the particle aspect ratio (ratio of the largest to the smallest particle dimensions). A morphological analysis of scanning electron microscope images of yellow desert dust particles performed by *Nakajima et al.* [1989] showed a distribution of aspect ratios about a mode of ~1.7. Unfortunately, *Nakajima et al.* [1989] did not describe the procedure for estimating aspect ratios of three-dimensional bodies based on measuring their two-dimensional projections and the method of statistical analysis. *Okada et al.* [1987] performed a similar study and found an average aspect ratio of two-dimensional particle projections close to 1.4, which implies that the aspect ratio for the original three-dimensional particles was close to 1.7, in good agreement with the result of *Nakajima et al.* [1989]. A more detailed and better documented study by *Hill et al.* [1984] showed that samples of soil particles could be represented by a mixture of prolate and oblate spheroids with a mode aspect ratio close to 2. However, in view of the relatively few published studies and the apparent uncertainties and differences, it is premature to conclude that definitive information on the aspect-ratio distribution of natural dustlike aerosols is already available. Therefore we decided to use in this paper the simplest, uniform distribution of aspect ratios centered at the aspect ratio 1.8 for both prolate and oblate spheroids. In other words, we assume that any aspect ratio in the shape distribution is equally probable and vary the width of the shape distribution by changing the minimum, $\varepsilon_{\min}$, and the maximum, $\varepsilon_{\max}$, aspect ratios such that $(\varepsilon_{\min} + \varepsilon_{\max})/2 = 1.8$. We have chosen the median aspect ratio $\varepsilon_{\text{med}} = 1.8$ to be in reasonable agreement with the above-mentioned laboratory estimates for yellow desert dust aerosols and soil particles. To further simplify computations, we have used only shape mixtures composed of a finite number of aspect ratios so that ε varies in discrete steps equal to $\Delta\varepsilon = 0.1$ or 0.2. Averaging over sizes and orientations makes the dependence of the phase function and the optical cross sections on the aspect ratio for polydisperse, randomly oriented spheroids rather smooth. As a consequence, our test computations have shown that the phase functions for aspect-ratio distributions with $\Delta\varepsilon = 0.2$ are essentially indistinguishable from equally wide distributions with $\Delta\varepsilon = 0.05$. We also assume that the size distribution of spheroids in a shape mixture is the same for all aspect ratios. Thus, using a quadrature formula for the numerical integration over the particle radii, we have the following formulas for computing the optical cross sections and the expansion coefficients for a shape mixture of polydisperse spheroids:

$$C_{\text{ext}} = \frac{1}{N_\varepsilon} \sum_{j=1}^{N_\varepsilon} \sum_{i=1}^{N} n(r_i)\, C_{\text{ext}}^{j}(r_i)\, w_i, \tag{15}$$

$$C_{\text{sca}} = \frac{1}{N_\varepsilon} \sum_{j=1}^{N_\varepsilon} \sum_{i=1}^{N} n(r_i)\, C_{\text{sca}}^{j}(r_i)\, w_i, \tag{16}$$

and

$$\omega_n = \frac{1}{N_\varepsilon C_{\text{sca}}} \sum_{j=1}^{N_\varepsilon} \sum_{i=1}^{N} n(r_i)\, \omega_n(r_i)\, C_{\text{sca}}^{j}(r_i)\, w_i, \tag{17}$$

where the index $j = 1, ..., N_\varepsilon$ numbers spheroid aspect ratios so that $\varepsilon_1 = \varepsilon_{\min}$ and $\varepsilon_{N_\varepsilon} = \varepsilon_{\max}$ and r_i and w_i ($i = 1, ..., N$) are quadrature division points and weights, respectively, on the interval $[r_{\min}, r_{\max}]$. The ensemble-averaged expansion coefficients ω_n are inserted in equation (7) to compute the corresponding phase function for an arbitrary set of scattering angles.

3. Results and Discussion

3.1. Phase Function for Particles of a Single Size

Plate 1 shows phase functions computed at two wavelengths corresponding to channels on the MISR instrument (λ = 443 and 865 nm) for polydisperse, randomly oriented prolate and oblate spheroids of a single shape. In these computations, we have used the size distribution for the standard model of the accumulation mode of dustlike aerosols given by equation (9) and refractive indices 1.53 + 0.0085i at 443 nm and 1.53 + 0.0012i at 865 nm [*Diner et al.*, 1994]. The respective spectral values of the effective size parameter for this distribution are 16.5 (443 nm) and 8.45 (865 nm). The spheroid aspect ratio ε varies from 1.2 (nearly spherically shaped particles) to 2.4 (highly aspherical particles). For comparison, the black curves show the phase functions for surface-equivalent polydisperse spheres. It is clear that the change of the phase function with increasing deviation of the particle shape from that of a sphere is gradual and highly systematic and is similar for prolate and oblate spheroids. Increasing the spheroid aspect ratio has two primary effects. First, it increases side-scattering at around Θ = 120°. Second, it reduces the backscattering phase function value $P(180°)$ (for $\varepsilon > 1.4$). However, the first effect significantly weakens, especially for prolate spheroids, and the second effect nearly saturates at aspect ratios larger than 2. Interestingly, all spheroidal phase functions show a significant backward peak as a rise of intensity at $\Theta = 180^{\circ}$ relative to that at Θ = 170°. *Wiscombe and Mugnai* [1988] note that for most laboratory setups for measuring light scattering by small particles the source-detector geometry precludes measurements past Θ = 170-175°, thus making the backward phase function peak hard to observe. This explains why many experimenters describe their phase functions as flat at backscattering angles compared to equivalent spheres. However, essentially all theoretical computations of light scattering for nonspherical particles with different degree of shape irregularity (e.g., Chebyshev particles [*Wiscombe and Mugnai*, 1988], spheroids [*Mishchenko et al.*, 1996a], finite circular cylinders [*Mishchenko et al.*, 1996b], bricks, hexagons, and tetrahedrons [*West et al.*, 1994] as well as microwave analog measurements [*Schuerman et al.*, 1981] suggest that the backward phase function peak can be a common property of both spherical and nonspherical particles. The forward-scattering phase function peak is almost independent of ε, thus substantiating the choice of the equal-projected-area-sphere radius to characterize the size of nonspherical particles.

The evolution of spherical-nonspherical differences with increasing aspect ratio and particle size relative to the wavelength can also be demonstrated by plotting the ratio ϱ of the nonspherical to spherical phase functions. Plate 2 shows $\varrho(\varepsilon)$ as a function of scattering angle Θ and effective size parameter $x_{\text{eff}} = 2\pi r_{\text{eff}}/\lambda$ for the power law size distribution of equation (11) with $v_{\text{eff}} = 0.2$. The refractive index is fixed at 1.53 + 0.008i, and the aspect ratio for both prolate and oblate spheroids varies from 1.2 to 2.2 in steps of 0.2. Note that the color bar in Plate 2 intentionally employs discrete colors so that visible boundaries between the colors facilitate the quantification of the respective color diagrams using the white regions as the reference. Plate 2 clearly shows the existence of a specific pattern which becomes fully developed for both prolate and oblate spheroids with aspect ratios exceeding 1.6 and consists of the following five distinct ϱ regions in order of increasing scattering angle.

Region 1
nonsphere $\approx$ sphere $0° \le \Theta \lesssim 10°$;
Region 2
nonsphere > sphere $10° \lesssim \Theta \lesssim 30°$;
Region 3
nonsphere < sphere $30° \lesssim \Theta \lesssim 90°$;
Region 4
nonsphere $\gg$ sphere $90° \lesssim \Theta \lesssim 150°$;
Region 5
nonsphere $\ll$ sphere $150° \lesssim \Theta \le 180°$.

Note that the scattering angle ranges indicated are nominal only and can change with particle size and shape. The first region is the region of exact forward scattering and is least sensitive to particle nonsphericity. As was mentioned above, this insensitivity is explained by our choice to characterize the size of randomly oriented spheroids using the radius of the sphere having the same projected area. The second region with $\varrho > 1$ becomes noticeable for aspect ratios larger than 1.5 and extends from about 10° to 30°. Region 3 with $\varrho < 1$ becomes more pronounced with aspect ratio increasing from 1 to about 2 and then weakens with further increasing ε. The right boundary of this region is highly aspect-ratio dependent and moves toward smaller scattering angles with increasing ε. In region 4, ϱ can well exceed 4 for oblate spheroids with aspect ratios about 1.6-1.8, thus indicating a strongly enhanced side-scattering as opposed to a deep and wide side-scattering minimum for spherical particles (cf. Plate 1). With increasing aspect ratio for both prolate and oblate spheroids, the left boundary of this region and the position of the maximum ϱ value shift toward smaller scattering angles. As in region 3, spherical-nonspherical differences in region 4 are greater for oblate than for prolate spheroids with the same aspect ratio and in most cases

increase with increasing effective size parameter. In the backscattering region, region 5, ϱ can drop below 0.25, thus indicating strongly suppressed backscattering. However, for prolate spheroids with aspect ratios smaller than 1.3 and for oblate spheroids with $\varepsilon < 1.5$ and effective size parameters larger than 10, the ϱ values at $\Theta = 180°$ can be greater than 1 and as large as 2, thereby generating a noticeable exception to the region 5 criterion $\varrho \ll 1$. Calculations of *Wiscombe and Mugnai* [1988] for moderately aspherical Chebyshev particles with size parameters exceeding 10 and computations of *Mishchenko et al.* [1996b] for polydisperse finite circular cylinders with effective size parameters exceeding 15 also show larger phase function values at $\Theta = 180°$ than those for equivalent spheres. This similarity is interesting, since, as opposed to the convex and entirely smooth surface of spheroids, Chebyshev particles are partially concave, while finite circular cylinders have sharp, rectangular edges.

3.2. Phase Functions for Shape Distributions of Spheroids

The upper panels in Plate 3 demonstrate the effect of increasing width of the spheroid shape distribution and show phase functions for equiprobable shape mixtures of spheroids with 2 (light blue curves, prolate and oblate spheroids with $\varepsilon = 1.8$) to 26 (red curves, prolate and oblate spheroids with aspect ratios ranging from 1.2 to 2.4 in steps of 0.1) components. These data were computed for the size distribution given by equation (9) and should be contrasted with phase functions for individual aspect ratios shown in Plate 1. For comparison, the black curves show the phase functions for projected-area-equivalent spherical particles. It is seen that with increasing width of the shape distribution the spheroidal phase functions become more and more featureless and show nearly flat side-scattering behavior or are mildly concave with a broad and shallow minimum centered at around 120-130°. In fact, the phase functions for the broadest shape distributions demonstrate nearly perfect resemblance to the phase functions measured for natural soil, yellow desert dust, and mineral particles (see Figure 6 of *Jaggard et al.* [1981], Figure 7 of *Nakajima et al.* [1989], Figure 6.6 of *Kuik* [1992], and *West et al.*, this issue).

The lower panels in Plate 3 show the phase functions averaged over all prolate (green curves) and oblate (blue curves) spheroids with aspect ratios ranging from 1.2 to 2.4 in steps of 0.1 as well as the phase functions for the mixture of all prolate and oblate spheroids (red curves). Importantly, despite the quite different shapes of prolate and oblate spheroids of the same aspect ratio, the green and blue curves lie rather close to one another. This suggests that the phase function of a representative shape mixture of nonspherical particles can be fairly insensitive to which elementary shapes are used to form the mixture. Figure 1 shows the ratios of the nonspherical to spherical phase functions denoted in the lower panels of Plate 3 as "all spheroids" and "spheres." Clearly, the greatest deviations of these ratios from unity are observed at side-scattering and near backscattering angles.

Figure 2 compares the phase function denoted as "all spheroids" in the lower left panel of Plate 3 and the phase function measured by *Jaggard et al.* [1981] for micron-sized soil particles. Although the theoretical computations pertain to the wavelength 443 nm whereas the measurements pertain to the wavelength 510 nm, the effective size parameters of the calculated and measured particles were close, as indicated by nearly the same values of the forward-scattering phase functions at $\Theta = 0°$. For comparison, Figure 2 also shows the phase function denoted as "spheres" in the lower left panel of Plate 3. It is seen that the theoretical phase function for the broad shape distribution of spheroids almost coincides with the phase function measured for natural soil particles. The residual differences between those phase functions are much smaller than the differences between either of them and the phase function computed for the equivalent spherical polydispersion. This result strongly indicates that (1) the smooth scattering-angle behavior of phase functions measured for samples of natural soil and dust particles can be caused by the samples being polydisperse mixtures of different particle shapes, and (2) the phase functions of natural nonspherical aerosols can be adequately modeled using a shape mixture of polydisperse, randomly oriented spheroids.

Plate 4 shows the ratio ϱ of the nonspherical to spherical phase functions versus scattering angle and effective size parameter for a shape mixture of prolate and oblate spheroids with aspect ratios ranging from 1.4 to 2.2 in steps of 0.2 and refractive index $1.53 + 0.008i$. These computations pertain to the power law size distribution of equation (11) with three values of the effective variance $v_{\mathrm{eff}} = 0.1$, 0.2, and 0.4. Since the maximum monodisperse size parameter for which convergent T-matrix computations for the most aspherical spheroids with $\varepsilon = 2.2$ are possible is equal to 49, the maximum effective size parameters for the three v_{eff} values are close to 30, 25, and 19 (see Table 1), thus dictating the successive shrinkage of the y axis range in Plate 4. It is seen that the ratio ϱ for the shape mixture fully preserves the specific scattering angle dependence described in Section 3.1. Spherical-nonspherical differences are significant for a wide size distribution with $v_{\mathrm{eff}} = 0.4$ and even slightly increase with decreasing v_{eff}. The evolution of spherical-nonspherical differences with increasing effective size parameter is also demonstrated in Plate 5, which shows the shape mixture and the projected-area-equivalent sphere phase functions for $v_{\mathrm{eff}} = 0.2$ and x_{eff} varying from 2 to 24 in steps of 2. In agreement with the experimental results of *Jaggard et al.* [1981], *Nakajima et al.* [1989], *Kuik* [1992], and *West et al.* [this issue], nonspherical phase functions are relatively featureless and show only a shallow minimum at side-scattering angles. This result is independent of the specific shape of the size distribution, as comparison of Plates 3 and 5 shows. Interestingly, the nonspherical phase function for $x_{\mathrm{eff}} = 4$ closely resembles the phase function computed by *West et al.* [1994] for a narrow lognormal size distribution of randomly oriented bricks (rectangular prisms with edges in the ratio 2:3:4) with $x_{\mathrm{eff}} = 4.29$. As opposed to smooth spheroids, the bricks are multifaceted particles with sharp rectangular edges.

Plates 3 and 4 show that nonspherical-spherical differences in the scattering phase function vanish or become small at scattering angles near 80-85° and 145-155°. This result may suggest that remote sensing measurements taken at these scattering angles are optimal for use in those cases when the real aerosols are nonspherical, but the aerosol optical thickness retrieval algorithm is based on Mie theory [cf.

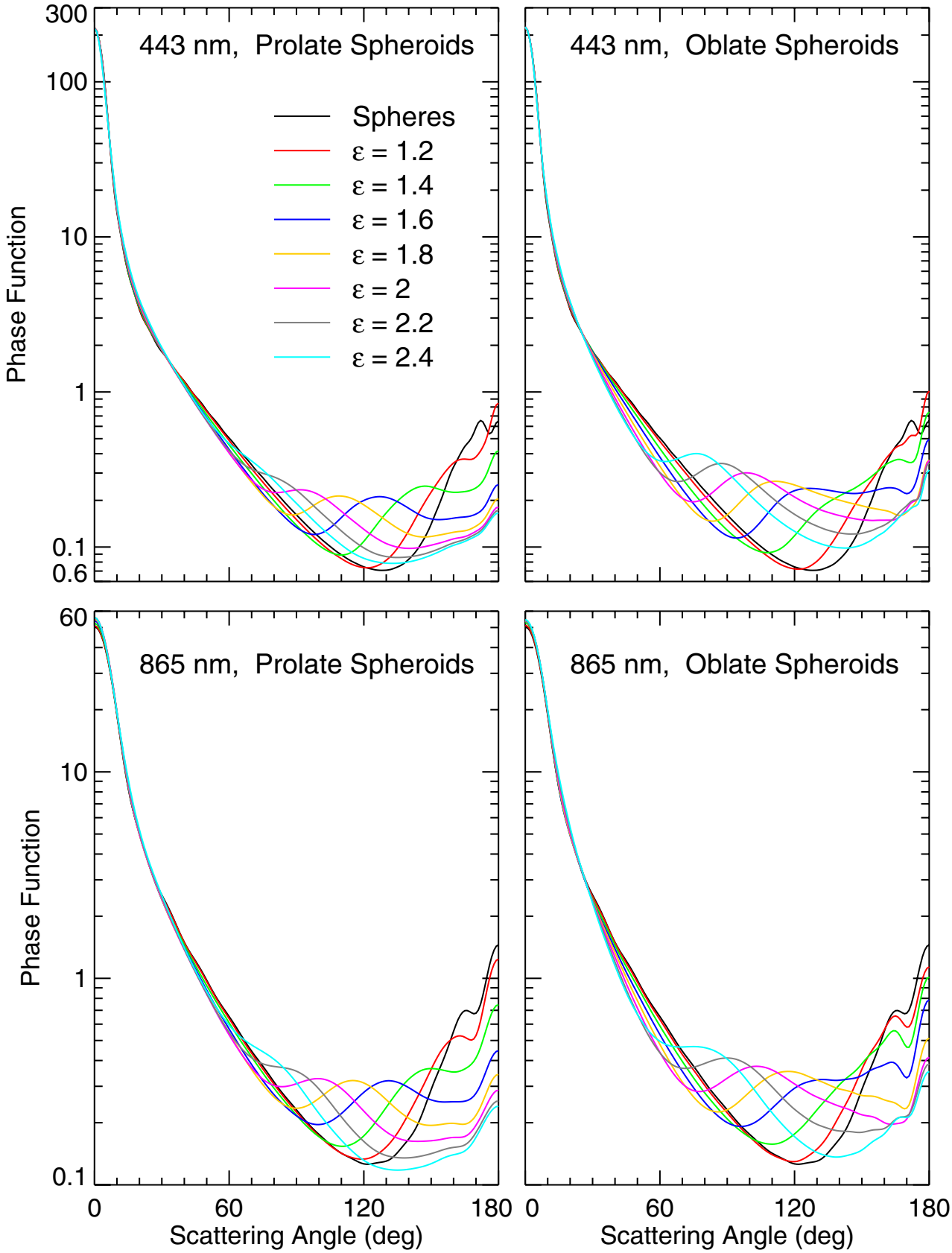

Plate 1. Phase functions for polydisperse, randomly oriented prolate and oblate spheroids with aspect ratios varying from 1 (spheres) to 2.4 (highly aspherical particles). The curves were computed for the modified lognormal distribution of surface-equivalent-sphere radii corresponding to the accumulation mode of dustlike tropospheric aerosols (equation (9)) at wavelengths 443 and 865 nm. The refractive indices are $1.53 + 0.0085i$ (443 nm) and $1.53 + 0.0012i$ (865 nm).

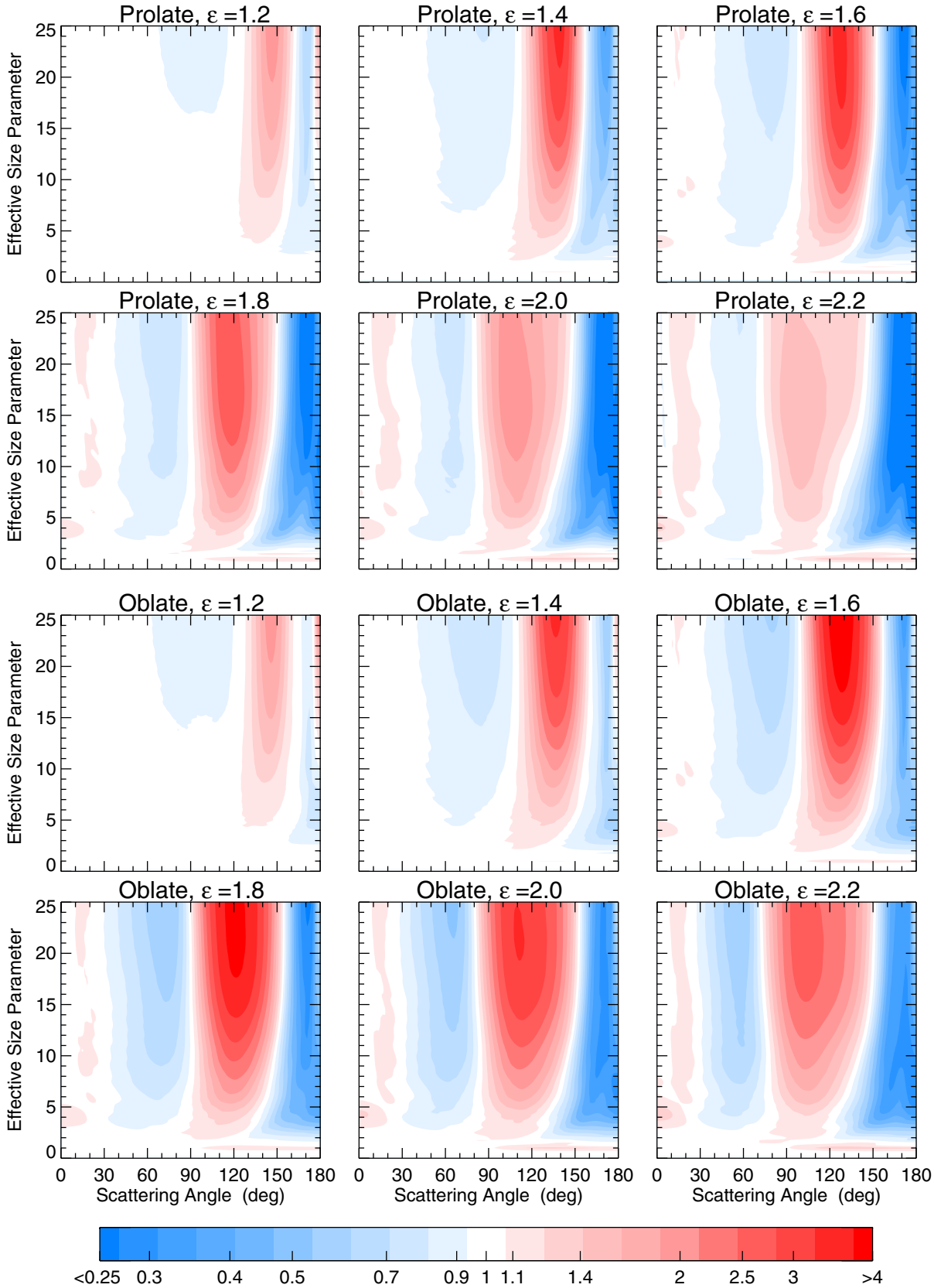

Plate 2. Ratio of the phase function of polydisperse, randomly oriented spheroids to that of surface-equivalent spheres versus scattering angle and effective size parameter. The data are shown for prolate and oblate spheroids with aspect ratios varying from 1.2 to 2.2 in steps of 0.2 and were computed assuming the power law size distribution given by equation (11) with effective variance $v_{\mathrm{eff}} = 0.2$. The refractive index is $1.53 + 0.008i$.

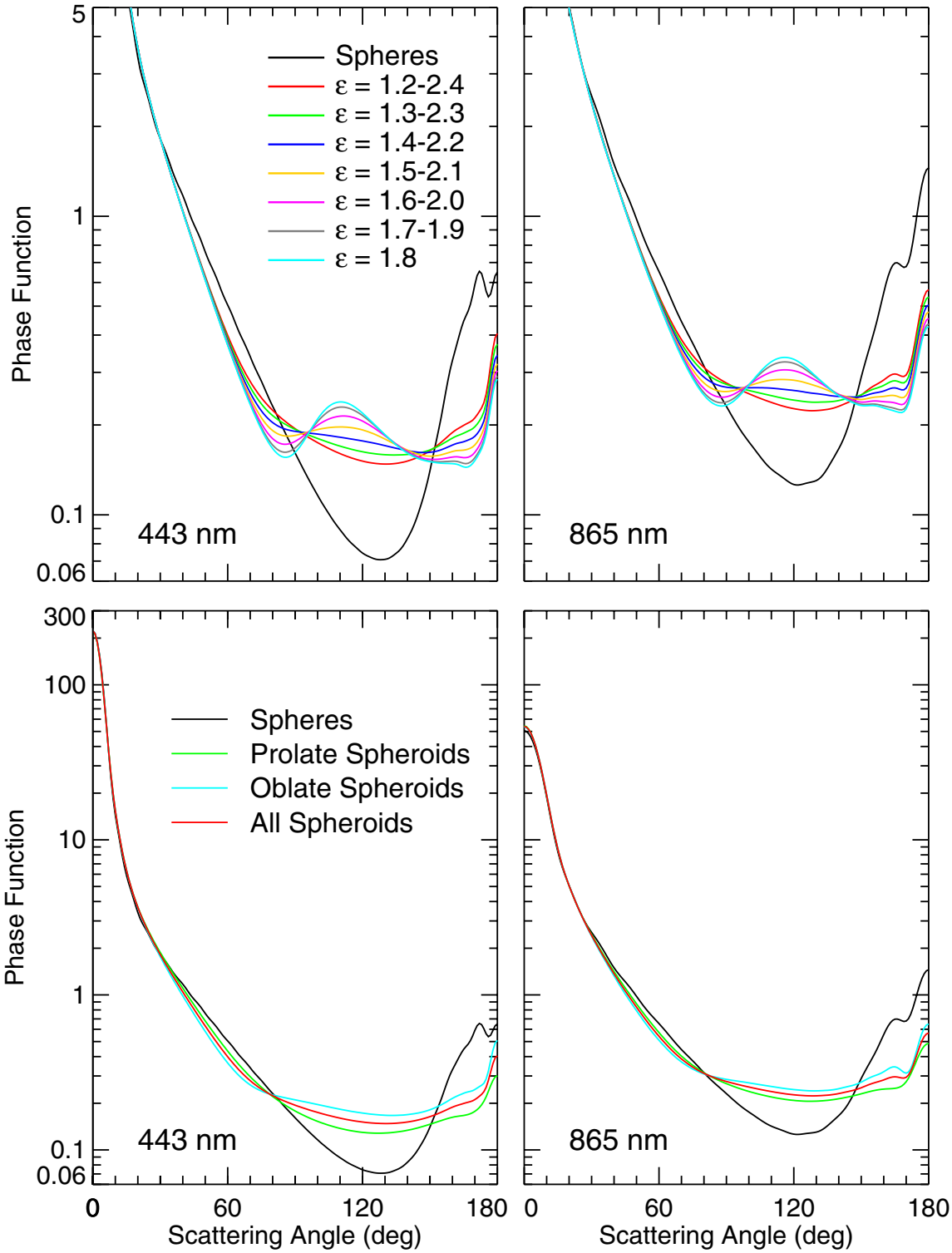

Plate 3. The upper panels demonstrate the effect of varying width of the spheroid aspect-ratio distribution and show ensemble-averaged phase functions for equiprobable shape mixtures of prolate and oblate spheroids with different aspect-ratio ranges. For all shape distributions the aspect-ratio step size is equal to 0.1. The lower panels show phase functions for polydisperse spheres and ensemble-averaged phase functions for equiprobable shape mixtures of prolate spheroids (green curve), oblate spheroids (blue curve), and prolate and oblate spheroids (red curve) with aspect ratios ranging from 1.2 to 2.4 in steps of 0.1. All curves were computed for the modified lognormal distribution of surface-equivalent-sphere radii corresponding to the accumulation mode of dustlike tropospheric aerosols (equation (9)) at wavelengths 443 and 865 nm. The spectral refractive indices are $1.53 + 0.0085i$ at 443 nm and $1.53 + 0.0012i$ at 865 nm.

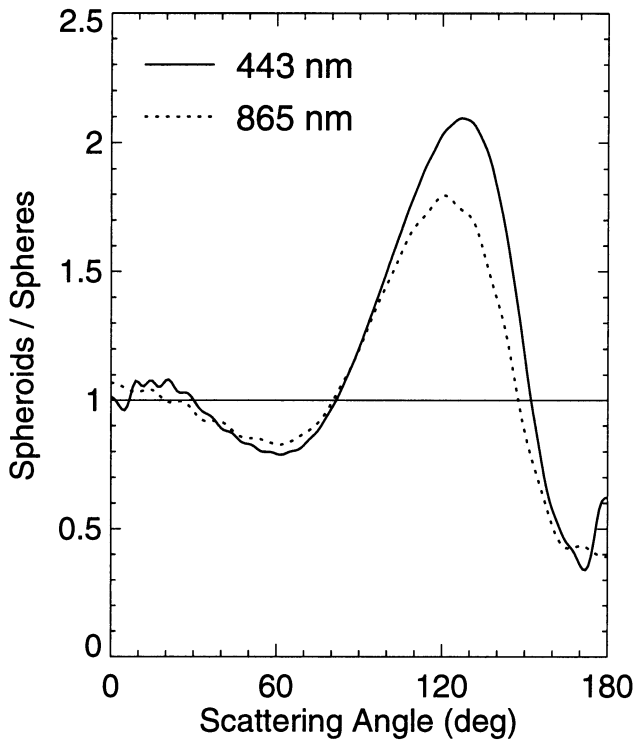

Figure 1. Ratios of the nonspherical to spherical phase functions denoted in lower panels of Plate 3 as "all spheroids" and "spheres."

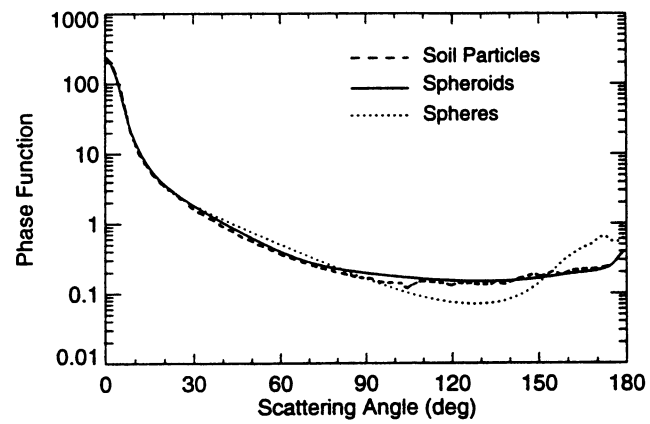

Figure 2. Scattering phase functions measured by *Jaggard et al.* [1981] for natural wavelength-sized soil particles and computed for a broad shape distribution of polydisperse, randomly oriented spheroids and surface-equivalent spheres.

Koepke and Quenzel, 1979; *Kaufman et al.*, this issue; *Kokhanovsky*, 1997].

The computations discussed so far pertain to moderately absorbing refractive indices of dust-like aerosols. One might expect that the effect of particle shape on scattering properties of nonspherical particles can become weaker with increasing imaginary part of the refractive index [*van de Hulst*, 1957; *Wiscombe and Mugnai*, 1986]. Recently, we

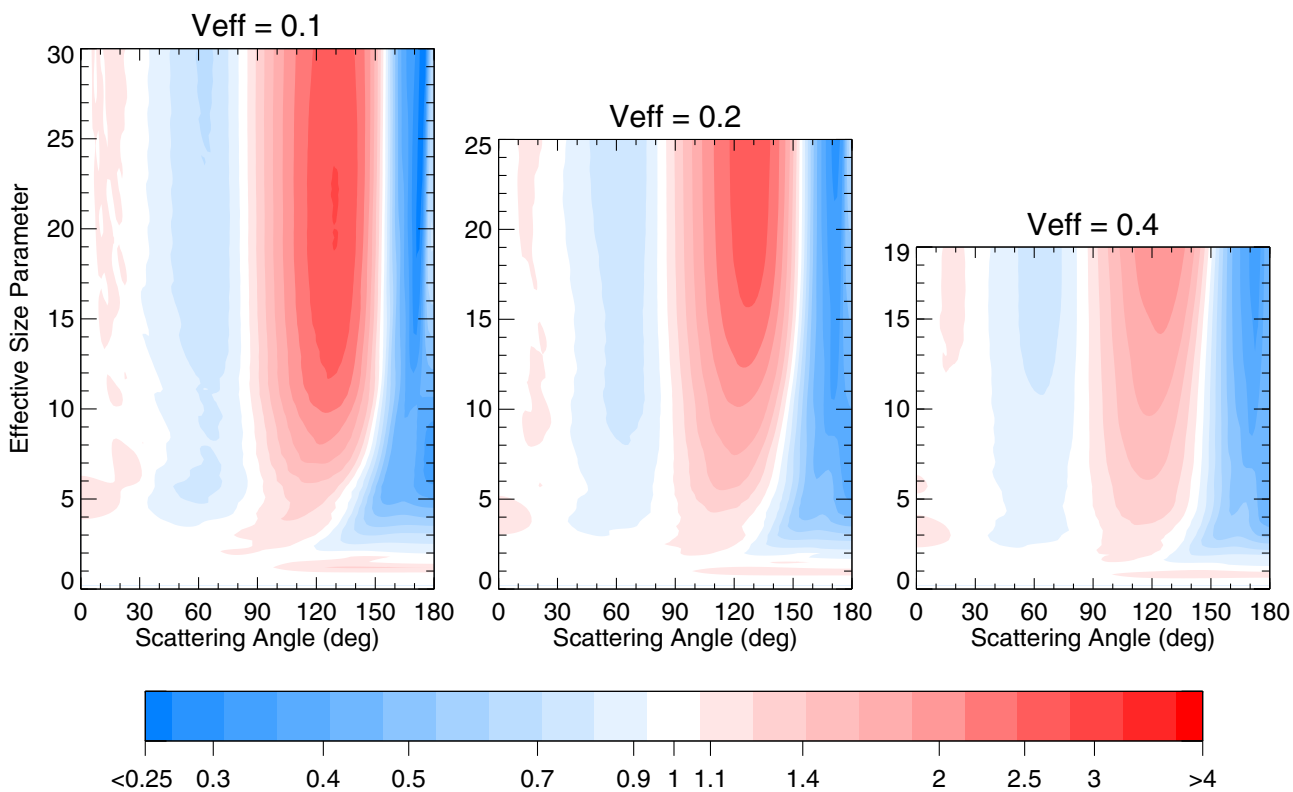

Plate 4. Ratio of the phase function for a polydisperse, equiprobable shape mixture of prolate and oblate spheroids with aspect ratios ranging from 1.4 to 2.2 in steps of 0.2 relative to that of surface-equivalent spheres versus scattering angle and effective size parameter x_{eff}. The data were computed assuming the power law size distribution given by equation (11) with effective variance values $v_{\mathrm{eff}} = 0.1$, 0.2, and 0.4. The refractive index is $1.53 + 0.008i$.

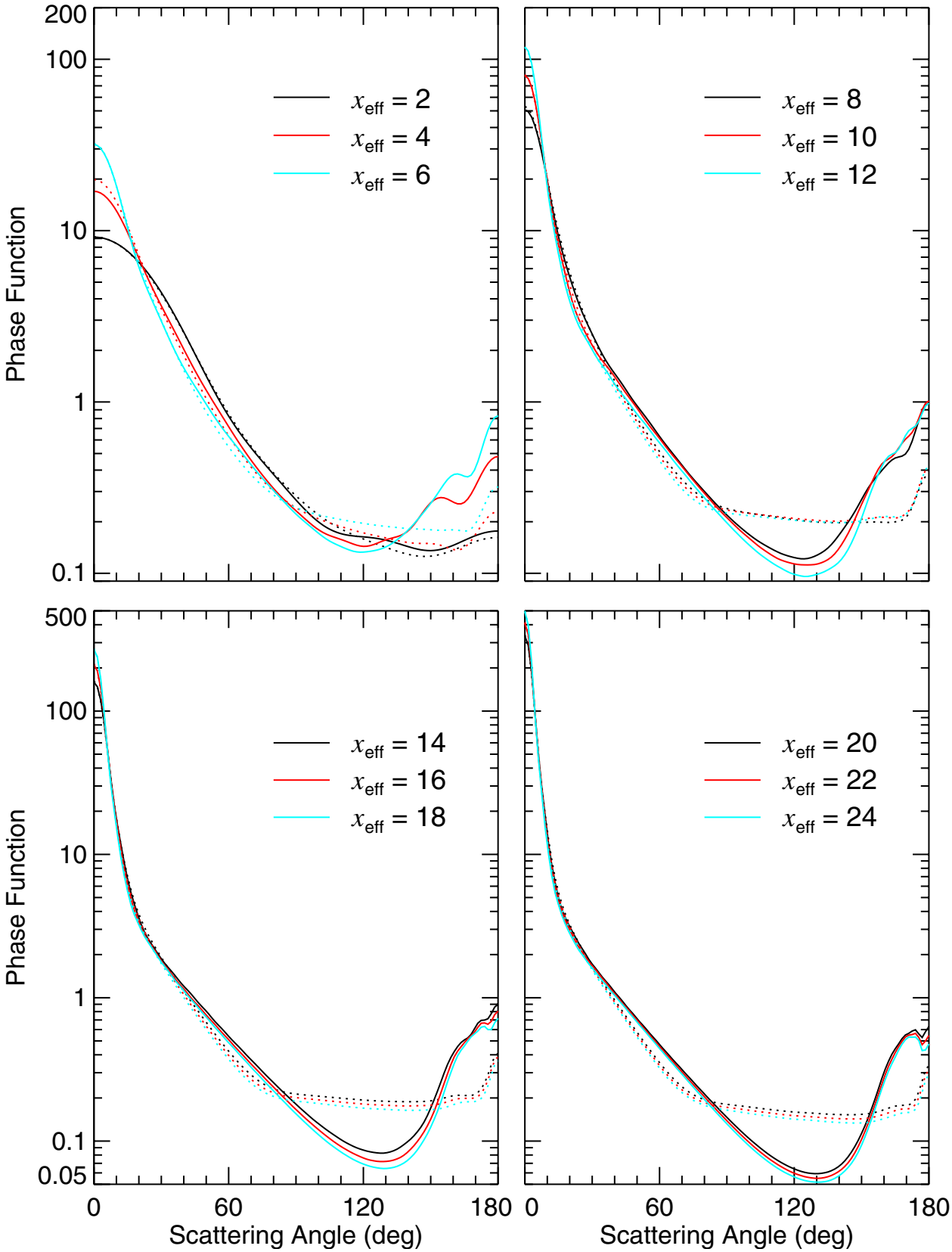

Plate 5. Phase functions for a polydisperse, equiprobable shape mixture of prolate and oblate spheroids with aspect ratios ranging from 1.4 to 2.2 in steps of 0.2 (dotted curves) and those for surface-equivalent spheres (solid curves) versus scattering angle for different values of the effective size parameter x_{eff}. The data were computed assuming the power law size distribution of equation (11) with effective variance v_{eff} = 0.2. The refractive index is 1.53 + 0.008i.

have shown that this is indeed true for the degree of linear polarization computed for polydisperse, randomly oriented spheroids [*Mishchenko and Travis*, 1994c]. Figure 3 shows the ratio of the nonspherical to spherical phase functions computed for a broad equiprobable shape distribution of spheroids (aspect ratios from 1.2 to 2.4 in steps of 0.1 for both prolate and oblate spheroids) and surface-equivalent spheres distributed over sizes according to equation (9). The wavelength is λ = 865 nm, and the real part of the refractive index is 1.53. It is clearly seen that nonspherical-spherical differences in the scattering phase function do decrease and eventually almost vanish as the imaginary part of the refractive index increases from 0.0005 to 0.5.

3.3. Total Cross Sections, Single-Scattering Albedo, Asymmetry Parameter, and Backscattered Fraction

Figures 4 to 9 show ratios of integral single-scattering characteristics (total optical cross sections, single-scattering albedo, asymmetry parameter of the phase function, and backscattered fraction) for polydisperse, equiprobable shape mixtures of prolate and oblate spheroids with aspect ratios ranging from 1.4 to 2.2 in steps of 0.2 relative to those for projected-area-equivalent spheres. These computations assume the power law distribution of equation (11) with v_{eff} = 0.1, 0.2, and 0.4 and the refractive index 1.5 + 0.008i. It is seen that spherical-nonspherical differences in the integral

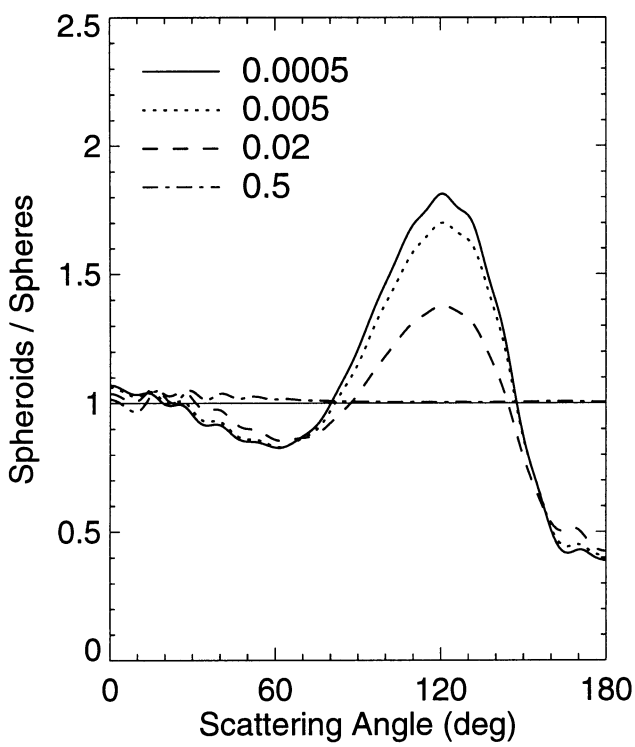

Figure 3. Ratio of the nonspherical to spherical phase functions computed for a broad shape distribution of spheroids (aspect ratios from 1.2 to 2.4 in steps of 0.1 for both prolate and oblate spheroids) and surface-equivalent spheres distributed over sizes according to equation (9). The wavelength is λ = 865 nm, the real part of the refractive index is 1.53, and the imaginary part of the refractive index is 0.0005, 0.005, 0.02, and 0.5.

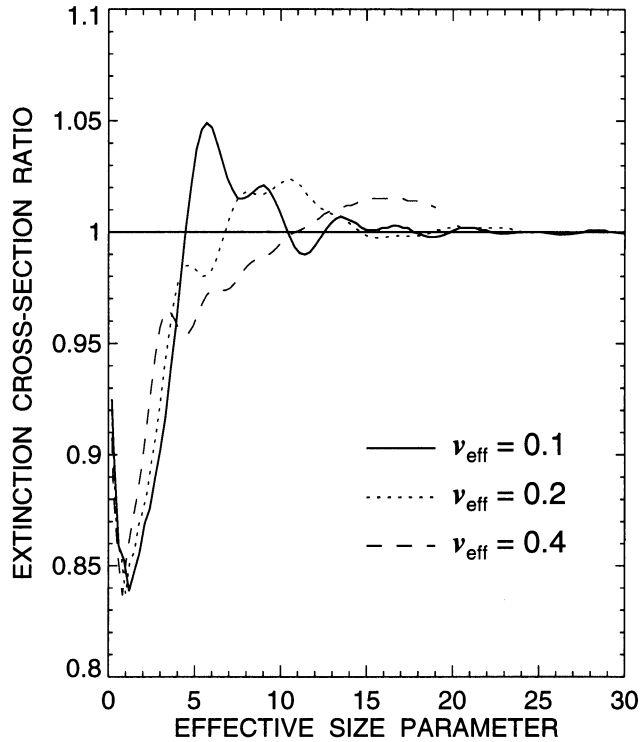

Figure 4. The ratio of the extinction cross section for a shape mixture of polydisperse, randomly oriented nonspherical aerosols relative to that for surface-equivalent spheres versus effective size parameter. The curves are computed assuming the power law size distribution with effective variance v_{eff} equal to 0.1, 0.2, and 0.4 and the equiprobable mixture of prolate and oblate spheroids with aspect ratios 1.4, 1.6, 1.8, 2, and 2.2. The refractive index is 1.53 + 0.008i.

single-scattering characteristics are significantly smaller than those in the phase functions. The differences are especially small for the single-scattering albedo at size parameters larger than about 1 (Figure 7). Interestingly, maximum spherical-nonspherical differences in the optical cross sections are observed at effective size parameters as small as 1-2 (Figures 4-6). Our computations for equal-volume spheres and spheroids suggest that this can be partially explained as the consequence of comparing scattering properties of projected-area-equivalent rather than volume-equivalent particles. On the other hand, the positive consequence of our choice of particle size characterization is that the asymptotic limit of 1 for the extinction cross-section ratio is essentially reached at size parameters as small as 12 (Figure 4).

Spherical-nonspherical differences in the asymmetry parameter of the phase function are less than ±7% in the entire range of effective size parameters from 0 to 30 and less than ±3.5% for x_{eff} larger than 7. It is important to note that similarly small differences follow from computations for randomly oriented Chebyshev particles [*Mugnai and Wiscombe*, 1986] and randomly oriented, polydisperse circular cylinders [*Mishchenko et al.*, 1996b]. These results may demonstrate the limited relevance of the semi-empirical theory of *Pollack and Cuzzi* [1980], which often predicts much smaller asymmetry parameters for

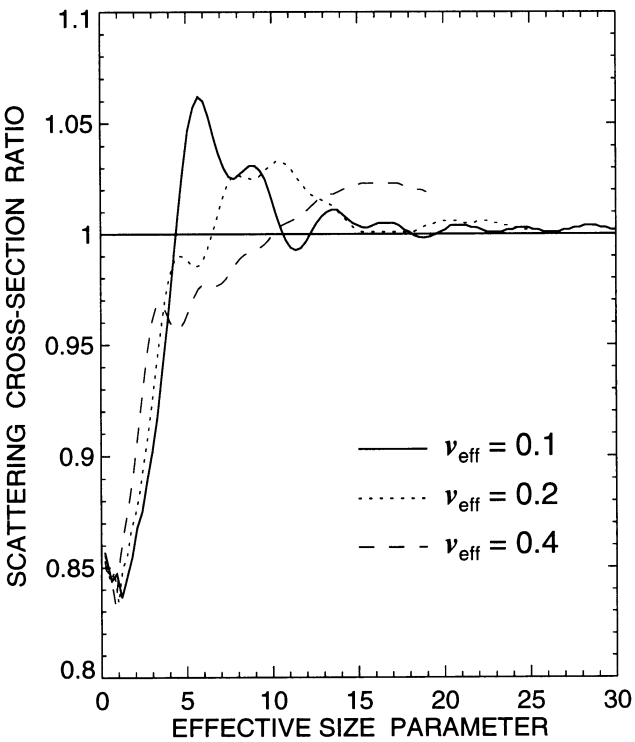

Figure 5. As in Figure 4, except for the ratio of the nonspherical to the spherical scattering cross sections.

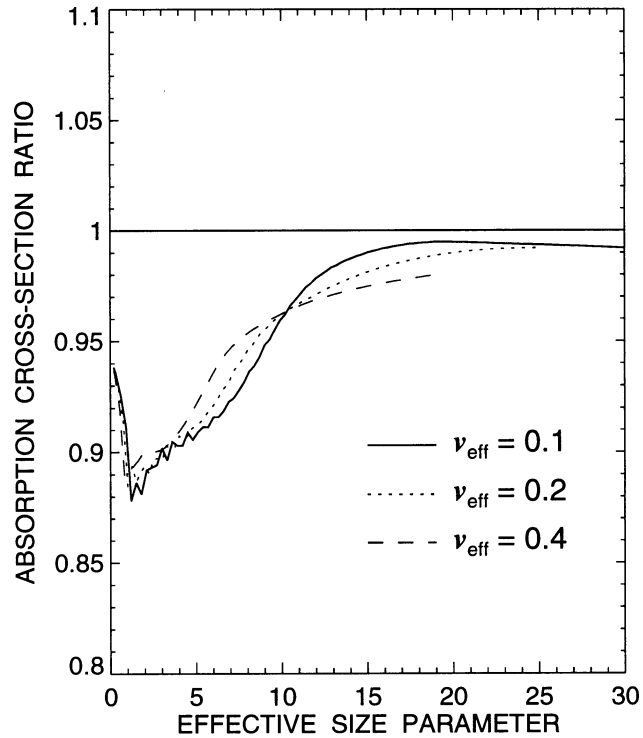

Figure 6. As in Figure 4, except for the ratio of the nonspherical to the spherical absorption cross sections.

wavelength-sized nonspherical particles than for equivalent spheres. Spherical-nonspherical differences in the backscattered fraction are also relatively small, especially at effective size parameters larger than 8 (Figure 9). An interesting feature of Figures 8 and 9 is that the asymmetry parameter and the backscattered fraction ratios are almost mirror images of one another with respect to the horizontal line at the level 1, i.e., for each x_{eff}, the larger the asymmetry parameter ratio the smaller the backscattered fraction ratio. This feature was first noted by *Mugnai and Wiscombe* [1986] in their computations for Chebyshev particles and then by *Mishchenko et al.* [1996b] in computations for polydisperse, finite, circular cylinders.

3.4. Extinction-to-Backscatter Ratio

The exact knowledge of the extinction-to-backscatter ratio R_{eb} for natural aerosol particles is very important in retrieving the aerosol optical thickness from lidar measurements because this ratio enters the so-called lidar equation [e.g., *Stephens*, 1994]. It is well known that for spherical particles, R_{eb} is extremely sensitive to the aerosol size and refractive index. Figure 10 shows the ratio of R_{eb} for the shape mixture of polydisperse spheroids relative to that for projected-area-equivalent spheres versus effective size parameter. As in Figures 4-9, we assume the power law size distribution of equation (11) with v_{eff} = 0.1, 0.2, and 0.4 and the refractive index 1.5 + 0.008i. The shape mixture is formed by prolate and oblate spheroids with aspect ratios ranging from 1.4 to 2.2 in steps of 0.2. The computations shown in Figure 10 clearly demonstrate that the extinction-to-backscatter ratio is highly sensitive not only to particle size and refractive index, but also to particle shape and even to the effective variance of the size distribution. The same conclusion was made by *Waggoner et al.* [1972], who

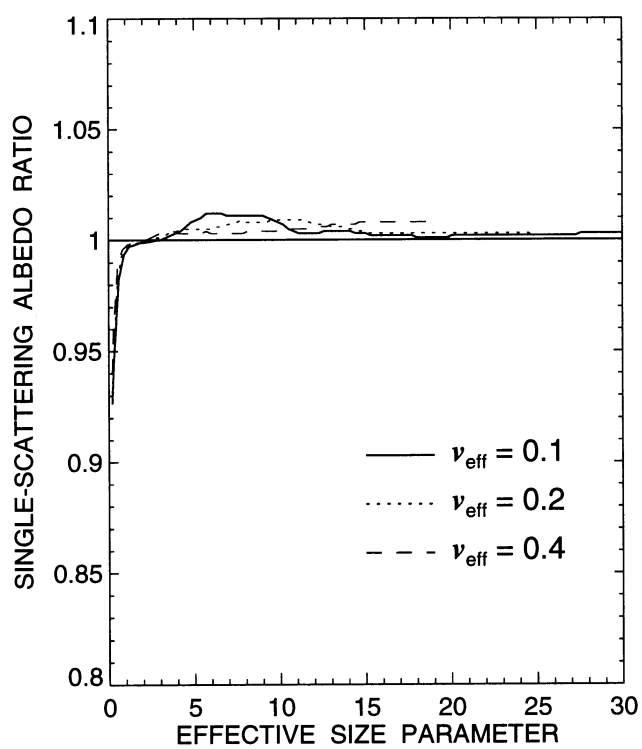

Figure 7. As in Figure 4, except for the ratio of the nonspherical to the spherical single-scattering albedos.

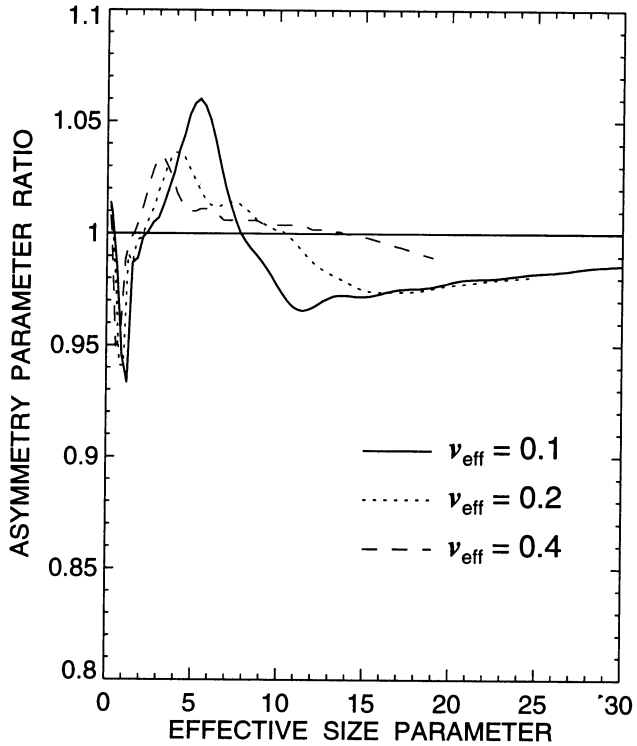

Figure 8. As in Figure 4, except for the ratio of the nonspherical to the spherical asymmetry parameters of the phase function.

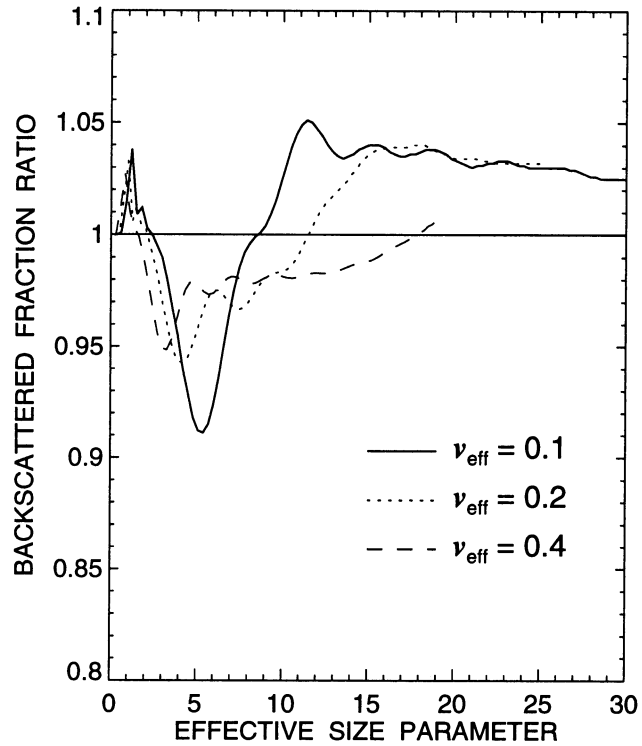

Figure 9. As in Figure 4, except for the ratio of the nonspherical to the spherical backscattered fractions.

measured R_{eb} for urban aerosols, *Sasano and Browell* [1989], who analyzed lidar measurements of Sahara dust aerosols, and by *Dungey and Bohren* [1993] on the basis of theoretical computations of backscattering by atmospheric ice crystals at radar frequencies. A qualitative physical explanation of the high sensitivity of backscattering to particle shape was given by *Bohren and Singham* [1991]. The inevitable consequence of this high sensitivity is that Mie theory is inapplicable both for calculating R_{eb} for nonspherical aerosols and for inverting lidar measurements for such particles.

4. Conclusions

This study was motivated by the need to provide a better representation of scattering properties of dustlike aerosols in the framework of the MISR and EOSP aerosol retrieval algorithm development. Since many laboratory and in situ measurements show that scattering properties of natural nonspherical particles can be significantly different from those of equivalent spheres, we decided to examine the feasibility of using rigorous T-matrix computations for simple spheroidal shapes to model scattering by natural dustlike aerosols. Our calculations have shown that a single spheroidal shape always produces a unique, shape-specific phase function distinctly different from those produced by other spheroidal shapes even after averaging over size distribution. However, phase functions averaged over a wide aspect-ratio distribution of prolate and oblate spheroids are smooth, featureless, and nearly flat at side-scattering angles and closely resemble those measured for natural soil and dust particles. Our results corroborate the main conclusion of *Hill et al.* [1984] that the scattering phase functions for natural soil and dust grains can be fairly well reproduced by particles which do not have sharp edges, surface roughness, or three-

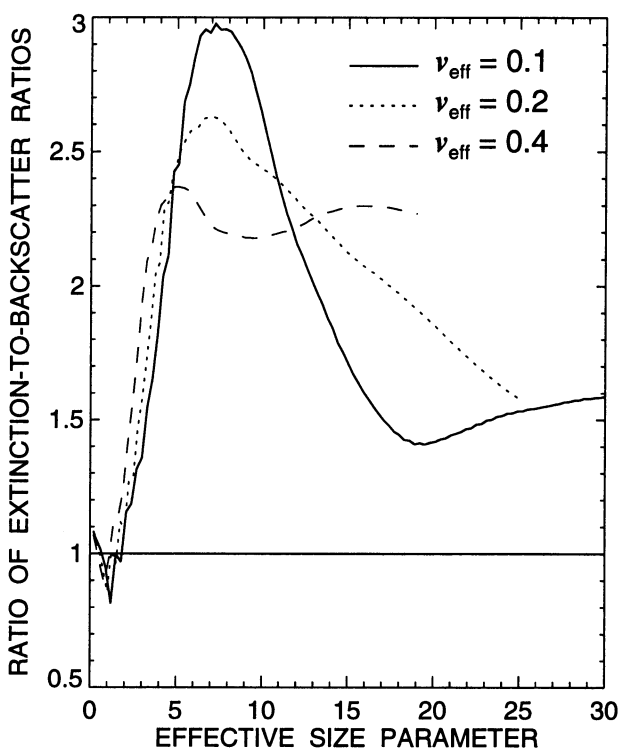

Figure 10. As in Figure 4, except for the ratio of the nonspherical to the spherical extinction-to-backscatter ratios.

dimensional asymmetries, and strongly suggest that the phase function of a representative shape mixture of nonspherical particles is fairly insensitive to what elementary shapes are used to form the mixture. Thus, although natural dust aerosols are surely not perfect spheroids, their phase function is always the result of averaging over a multitude of different shapes and apparently can be adequately modeled using a wide aspect-ratio distribution of prolate and oblate spheroidal particles.

Our computations for nonspherical versus projected-area-equivalent spherical particles show that spherical-nonspherical differences in the scattering phase function are large, especially at side-scattering and backscattering angles. Therefore one should expect possibly significant errors in the retrieved aerosol optical thickness if Mie theory is used to analyze reflectance measurements for nonspherical aerosols [*Mishchenko et al.*, 1995]. In contrast, the differences in the total optical cross sections, single-scattering albedo, and backscattered fraction are much smaller and in most cases do not exceed a few percent. This result suggests that the influence of particle shape on the aerosol radiative forcing can be negligibly small and can be accurately computed using Mie theory provided that the aerosol optical thickness is already known [*Lacis and Mishchenko*, 1995; *Mishchenko et al.*, 1995]. (Note that the latter conclusion was made on the basis of adding/doubling computations of radiative transfer. However, recently C. Pilinis and X. Li (personal communication) have used a box model [*Charlson et al.*, 1991; *Pilinis et al.*, 1995] and derived a potentially rather strong effect of particle nonsphericity on the direct aerosol forcing of climate.) It is important to emphasize, however, that no cancellation of errors occurs if one consistently uses Mie theory in retrieving the dustlike aerosol optical thickness and then in computing the aerosol radiative forcing for the retrieved optical thickness value [*Mishchenko et al.*, 1995]. Spherical-nonspherical differences in the extinction-to-backscatter ratio are dominated by the differences in the backscattering phase function and can exceed a few hundred percent. Therefore particle nonsphericity should be explicitly taken into account in inverting lidar measurements of dustlike aerosols.

Finally, we note that all our results pertain to a specific refractive index typical of dustlike tropospheric aerosols. Therefore our conclusions should not be straightforwardly extrapolated to other values of the refractive index without additional extensive calculations and laboratory measurements.

Acknowledgments. We thank B. E. Carlson and A. A. Lacis for many valuable discussions, J. W. Hovenier and anonymous referees for careful and constructive reviews, and N. T. Zakharova for help with graphics. This research was funded by the Earth Observing Project managed by Goddard Space Flight Center and was performed at the NASA Goddard Institute for Space Studies and at the Jet Propulsion Laboratory, California Institute of Technology under contract with the National Aeronautics and Space Administration.

References

Bohren, C. F., and D. R. Huffman, *Absorption and Scattering of Light by Small Particles*, John Wiley, New York, 1983.

Bohren, C. F., and S. B. Singham, Backscattering by nonspherical particles: A review of methods and suggested new approaches, *J. Geophys. Res.*, *96*, 5269-5277, 1991.

Charlson, R. J., J. Langner, H. Rodhe, C. B. Leovy, and S. G. Warren, Perturbation of the northern hemisphere radiative balance by backscattering from anthropogenic sulfate aerosols, *Tellus*, *43AB*, 152-163, 1991.

Charlson, R. J., S. E. Schwartz, J. M. Hales, R. D. Cess, J. A. Coakley, J. E. Hansen, and D. J. Hoffman, Climate forcing by anthropogenic aerosols, *Science*, *255*, 423-430, 1992.

Deschamps, P.-Y., F.-M. Bréon, M. Leroy, A. Podaire, A. Bricaud, J.-C. Buriez, and G. Séze, The POLDER mission: Instrument characteristics and scientific objectives, *IEEE Trans. Geosci. Remote Sens.*, *32*, 598-615, 1994.

Diner, D. J., C. J. Bruegge, J. V. Martonchik, G. W. Bothwell, E. D. Danielson, E. L. Floyd, V. G. Ford, L. E. Hovland, K. L. Jones, and M. L. White, A Multi-angle Imaging SpectroRadiometer for terrestrial remote sensing from the Earth Observing System, *Int. J. Imaging Syst. Technol.*, *3*, 92-107, 1991.

Diner, D. J., W. Abdou, T. Ackerman, J. Conel, H. Gordon, R. Kahn, J. Martonchik, S. Paradise, M. Wang, and R. West, MISR level 2 algorithm theoretical basis: Aerosol/surface product, part 1 (aerosol parameters), Rep. *JPL-D11400*, Rev. A, Jet Propul. Lab., Pasadena, Calif., 1994.

Draine, B. T., and P. J. Flatau, Discrete-dipole approximation for scattering calculations, *J. Opt. Soc. Am. A*, *11*, 1491-1499, 1994.

Dungey, C. E., and C. F. Bohren, Backscattering by nonspherical hydrometeors as calculated by the coupled-dipole method: An application in radar meteorology, *J. Atmos. Ocean. Technol.*, *10*, 526-532, 1993.

Francis, P. N., Some aircraft observations of the scattering properties of ice crystals, *J. Atmos. Sci.*, *52*, 1142-1154, 1995.

Gayet, J.-F., O. Crépel, and J.-F. Fournol, A new polar nephelometer for in situ measurements of microphysical and optical properties of clouds, in *Proceedings of the Conference on Cloud Physics*, pp. 26-30, Am. Meteorol. Soc., Boston, Mass., 1995.

Guieu, C., R. Duce, and R. Arimoto, Dissolved input of manganese to the ocean: aerosol source, *J. Geophys. Res.*, *99*, 18789-18800, 1994.

Hansen, J. E., and J. W. Hovenier, Interpretation of the polarization of Venus, *J. Atmos. Sci.*, *31*, 1137-1160, 1974.

Hansen, J. E., and A. A. Lacis, Sun and dust versus greenhouse gases: An assessment of their relative roles in global climate change, *Nature*, *346*, 713-719, 1990.

Hansen, J. E., and L. D. Travis, Light scattering in planetary atmospheres, *Space Sci. Rev.*, *16*, 527-610, 1974.

Hansen, J., W. Rossow, B. Carlson, A. Lacis, L. Travis, A. DelGenio, I. Fung, B. Cairns, M. Mishchenko, and M. Sato, Low-cost long-term monitoring of global climate forcings and feedbacks, *Clim. Change*, *31*, 247-271, 1995.

Heintzenberg, J., Particle size distributions from scattering measurements of nonspherical particles via Mie-theory, *Beitr. Phys. Atmos.*, *51*, 91-99, 1978.

Hill, S. C., A. C. Hill, and P. W. Barber, Light scattering by size/shape distributions of soil particles and spheroids, *Appl. Opt.*, *23*, 1025-1031, 1984.

Jaggard, D. L., C. Hill, R. W. Shorthill, D. Stuart, M. Glantz, F. Rosswog, B. Taggard, and S. Hammond, Light scattering from particles of regular and irregular shape, *Atmos. Environ.*, *15*, 2511-2519, 1981.

Kahn, R., R. West, W. Abdou, D. McDonald, B. Rheingans, and M. Mishchenko, Sensitivity of multi-angle remote sensing to aerosol sphericity, *J. Geophys. Res.*, this issue.

Kaufman, Y. J., Aerosol optical thickness and atmospheric path radiance, *J. Geophys. Res.*, *98*, 2677-2692, 1993.

Kaufman, Y. J., D. Tanré, L. A. Remer, E. F. Vermote, A. Chu, and B. N. Holben, Operational remote sensing of tropospheric aerosol over the land from EOS moderate resolution imaging spectroradiometer, *J. Geophys. Res.*, this issue.

King, M. D., Y. J. Kaufman, W. P. Menzel, and D. Tanré, Remote sensing of cloud, aerosol, and water vapor properties from the Moderate Resolution Imaging Spectrometer (MODIS), *IEEE Trans. Geosci. Remote Sens.*, *30*, 2-27, 1992.

Koepke, P., and M. Hess, Scattering functions of tropospheric aerosols: The effects of nonspherical particles, *Appl. Opt.*, *27*, 2422-2430, 1988.

Koepke, P., and H. Quenzel, Turbidity of the atmosphere determined from satellite: Calculation of optimum viewing geometry, *J. Geophys. Res.*, *84*, 7847-7856, 1979.

Kokhanovsky, A. A., On variability of phase function of atmospheric aerosols at large scattering angles, *J. Atmos. Sci.*, in press, 1997.

Kuik, F., Single scattering of light by ensembles of particles with various shapes, Ph.D. thesis, Free Univ., Amsterdam, 1992.

Kuik, F., J. F. de Haan, and J. W. Hovenier, Single scattering of light by circular cylinders, *Appl. Opt.*, *33*, 4906-4918, 1994.

Lacis, A. A., and M. I. Mishchenko, Climate forcing, climate sensitivity, and climate response: A radiative modeling perspective on atmospheric aerosols, in *Aerosol Forcing of Climate*, edited by R. J. Charlson and J. Heintzenberg, pp. 11-42, John Wiley, New York, 1995.

Lacis, A., J. E. Hansen, and M. Sato, Climate forcing by stratospheric aerosols, *Geophys. Res. Lett.*, *19*, 1607-1610, 1992.

Lenoble, J., and C. Brogniez, A comparative review of radiation aerosol models, *Beitr. Phys. Atmos.*, *57*, 1-20, 1984.

Lumme, K., and J. Rahola, Light scattering by porous dust particles in the discrete-dipole approximation, *Astrophys. J.*, *425*, 653-667, 1994.

Macke, A., Scattering of light by polyhedral ice crystals, *Appl. Opt.*, *32*, 2780-2788, 1993.

Macke, A., J. Mueller, and E. Raschke, Single scattering properties of atmospheric ice crystals, *J. Atmos. Sci.*, *53*, 2813-2825, 1996.

Marshall, S. F., D. S. Covert, and R. J. Charlson, Relationship between asymmetry parameter and hemispheric backscatter ratio: Implications for climate forcing by aerosols, *Appl. Opt.*, *34*, 6306-6311, 1995.

Mishchenko, M. I., Light scattering by randomly oriented axially symmetric particles, *J. Opt. Soc. Am. A*, *8*, 871-882, 1991.

Mishchenko, M. I., Light scattering by size-shape distributions of randomly oriented axially symmetric particles of a size comparable to a wavelength, *Appl. Opt.*, *32*, 4652-4666, 1993.

Mishchenko, M. I., and L. D. Travis, T-matrix computations of light scattering by large spheroidal particles, *Opt. Commun.*, *109*, 16-21, 1994a.

Mishchenko, M. I., and L. D. Travis, Light scattering by polydispersions of randomly oriented spheroids with sizes comparable to wavelengths of observation, *Appl. Opt.*, *33*, 7206-7225, 1994b.

Mishchenko, M. I., and L. D. Travis, Light scattering by polydisperse, rotationally symmetric nonspherical particles: Linear polarization, *J. Quant. Spectrosc. Radiat. Transfer*, *51*, 759-778, 1994c.

Mishchenko, M. I., A. A. Lacis, B. E. Carlson, and L. D. Travis, Nonsphericity of dust-like tropospheric aerosols: Implications for aerosol remote sensing and climate modeling, *Geophys. Res. Lett.*, *22*, 1077-1080, 1995.

Mishchenko, M. I., L. D. Travis, and D. W. Mackowski, *T*-matrix computations of light scattering by nonspherical particles: A review, *J. Quant. Spectrosc. Radiat. Transfer*, *55*, 535-575, 1996a.

Mishchenko, M. I., L. D. Travis, and A. Macke, Scattering of light by polydisperse, randomly oriented, finite circular cylinders, *Appl. Opt.*, *35*, 4927-4940, 1996b.

Mugnai, A., and W. J. Wiscombe, Scattering from nonspherical Chebyshev particles, 1, Cross sections, single-scattering albedo, asymmetry factor, and backscattered fraction, *Appl. Opt.*, *25*, 1235-1244, 1986.

Muinonen, K., K. Lumme, J. Peltoniemi, and W. M. Irvine, Light scattering by randomly oriented crystals, *Appl. Opt.*, *28*, 3051-3060, 1989.

Nakajima, T., M. Tanaka, M. Yamano, M. Shiobara, K. Arao, and Y. Nakanishi, Aerosol optical characteristics in the yellow sand events observed in May, 1982 at Nagasaki, II, Models, *J. Meteorol. Soc. Jpn.*, *67*, 279-291, 1989.

Okada, K., A. Kobayashi, Y. Iwasaka, H. Naruse, T. Tanaka, and O. Nemoto, Features of individual asian dust-storm particles collected at Nagoya, Japan, *J. Meteorol. Soc. Jpn.*, *65*, 515-521, 1987.

Perry, R. J., A. J. Hunt, and D. R. Huffman, Experimental determinations of Mueller scattering matrices for nonspherical particles, *Appl. Opt.*, *17*, 2700-2710, 1978.

Pilinis, C., S. N. Pandis, and J. H. Seinfeld, Sensitivity of direct climate forcing by atmospheric aerosols to aerosol size and composition, *J. Geophys. Res.*, *100*, 18,739-18,754, 1995.

Pollack, J. B., and J. N. Cuzzi, Scattering by nonspherical particles of size comparable to a wavelength: A new semi-empirical theory and its application to tropospheric aerosols, *J. Atmos. Sci.*, *37*, 868-881, 1980.

Posse, P., and W. von Hoyningen-Huene, Information about scattering properties and particle characteristics of a stratiform cloud at Helgoland by remote optical measurements, *Beitr. Phys. Atmos.*, *68*, 359-366, 1995.

Reagan, J. A., M. P. McCormick, and J. D. Spinhirne, Lidar sensing of aerosols and clouds in the troposphere and stratosphere, *Proc. IEEE*, *77*, 433-448, 1989.

Sasano, Y., and E. V. Browell, Light scattering characteristics of various aerosol types derived from multiple wavelength lidar observations, *Appl. Opt.*, *28*, 1670-1679, 1989.

Schuerman, D. W., R. T. Wang, B. Å. S. Gustafson, and R. W. Schaefer, Systematic studies of light scattering. 1: Particle shape, *Appl. Opt.*, *20*, 4039-4050, 1981.

Stephens, G. L., *Remote Sensing of the Lower Atmosphere*, Oxford Univ. Press, New York, 1994.

Takano, Y., and K.-N. Liou, Solar radiative transfer in cirrus clouds, 1, Single-scattering and optical properties of hexagonal ice crystals, *J. Atmos. Sci.*, *46*, 3-19, 1989.

Toon, O. B., and J. B. Pollack, A global model of atmospheric aerosols for radiative transfer calculations, *J. Appl. Meteorol.*, *15*, 225-246, 1976.

Travis, L. D., Remote sensing of aerosols with the Earth Observing Scanning Polarimeter, in *Polarization and Remote Sensing*, edited by W. G. Egan, *Proc. SPIE, Int. Soc. Opt. Eng.*, *1747*, 154-164, 1992.

van de Hulst, H. C., *Light Scattering by Small Particles*, 470 pp., John Wiley, New York, 1957.

van de Hulst, H. C., *Multiple Light Scattering*, 739 pp., Academic, San Diego, Calif., 1980.

von Hoyningen-Huene, W., and M. Wendisch, Variability of aerosol optical parameters by advective processes, *Atmos. Environ.*, *28*, 923-933, 1994.

Waggoner, A. P., N. C. Ahlquist, and R. J. Charlson, Measurement of the aerosol total scatter-backscatter ratio, *Appl. Opt.*, *11*, 2886-2889, 1972.

Wang, M., and H. R. Gordon, Estimating aerosol optical properties over the oceans with the multiangle imaging spectroradiometer: Some preliminary results, *Appl. Opt.*, *33*, 4042-4057, 1994.

Waterman, P. C., Symmetry, unitarity, and geometry in electromagnetic scattering, *Phys. Rev. D*, *3*, 825-839, 1971.

West, R. A., M. G. Tomasko, and L. R. Doose, Optical properties of small mineral dust particles at visible-near-IR wavelengths: Numerical calculations and laboratory measurements, in *Eighth Conference on Atmospheric Radiation, Nashville, Tennessee, January 23-28, 1994*, pp. 341-343, Am. Meteorol. Soc., Boston, Mass., 1994.

West, R., L. Doose, A. Eibl, M. Tomasko, and M. Mishchenko, Laboratory measurements of mineral dust scattering phase function and linear polarization, *J. Geophys. Res.*, this issue.

Wielaard, D. J., M. I. Mishchenko, A. Macke, and B. E. Carlson, Improved *T*-matrix computations for large, nonabsorbing and weakly absorbing nonspherical particles and comparison with geometric optics approximation, *Appl. Opt.*, accepted, 1997.

Wiscombe, W. J., and G. W. Grams, The backscattered fraction in two-stream approximations, *J. Atmos. Sci.*, *33*, 2440-2451, 1976.

Wiscombe, W. J., and A. Mugnai, Single scattering from nonspherical Chebyshev particles: A compendium of calculations, *NASA Ref. Publ.*, *1157*, 1986.

Wiscombe, W. J., and A. Mugnai, Scattering from nonspherical Chebyshev particles, 2, Means of angular scattering patterns, *Appl. Opt.*, *27*, 2405-2421, 1988.

R. A. Kahn and R. A. West, Jet Propulsion Laboratory, California Institute of Technology, 4800 Oak Grove Drive, Pasadena, CA 91109. (e-mail: kahn@jord.jpl.nasa.gov; raw@west.jpl.nasa.gov)

M. I. Mishchenko and L. D. Travis, NASA Goddard Institute for Space Studies, 2880 Broadway, New York, NY 10025. (e-mail: crmim@giss.nasa.gov; pdldt@giss.nasa.gov)

(Received January 22, 1996; revised June 18, 1996; accepted June 18, 1996.)